Project: **620**
Project title: **Vertical Propagation of Gravity Waves into the Middle Atmosphere**
Project lead: **Andreas Dörnbrack**
Report period: **2019-01-01 to 2019-12-31**

In the reporting period, the computer time was mainly used to conduct simulations of mountain wave events which were observed during airborne campaigns as NAWDEX (Schäfler et. al., 2018), and for a selected deep mountain wave propagation event from DEEPWAVE (Fritts et al., 2016). The simulations are tied closely to the atmospheric conditions encountered during the field measurements. This strategy enabled the interpretation of measurement data by means of involved important processes. The first part of this report presents numerical simulations conducted for an observed clear-air turbulence event encountered by the High Altitude and Long Range Research Aircraft (HALO) over the Iceland during NAWDEX (Bramberger et al., 2019). The physical conditions that led to moderate and severe turbulence encountered by HALO are investigated. The second part of this report focuses on the reanalysis of an observed event during DEEPWAVE where ship-wave-like patterns were observed directly above the Southern Ocean Auckland Islands but in about 87 km altitude. The reasons for these surprisingly deep vertical modes are here studied by 2D simulations. Currently, 3D simulations are set up and will be conducted during the next year.

Breaking Mountain Wave over Iceland

During the recent NAWDEX campaign (Schäfler et al., 2019), strong turbulence was encountered by the German High Altitude Long range research aircraft (HALO) at FL 430 (13.8 km) on 13 October 2016 above Iceland. In this event the turbulence caused altitude changes of the research aircraft of about 50 m within a period of approximately 15 s. Additionally, the automatic thrust control of the HALO could not control the large gradients in the horizontal wind speed and, consequently, the pilot had to switch off this system. Simultaneously, the French Falcon of Safire, flying 2 km below HALO, also encountered turbulence at almost the same location.

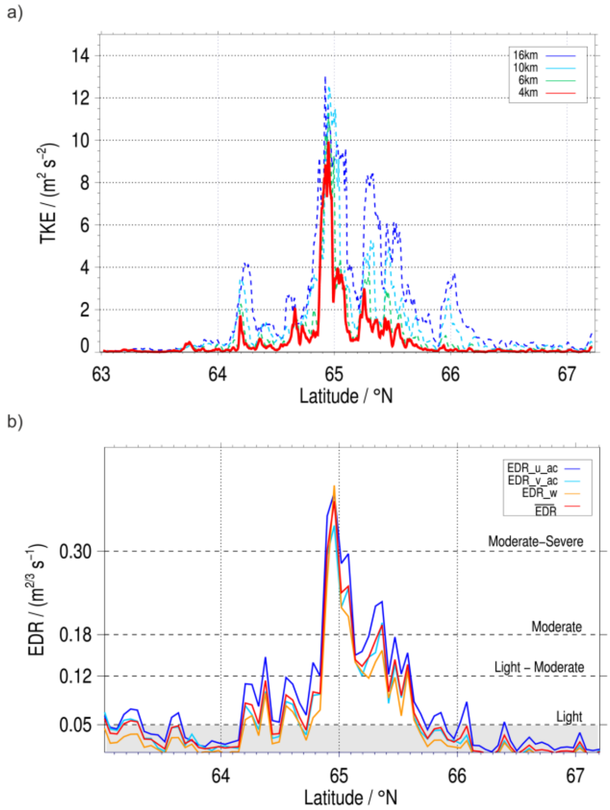

Figure 1: (a) Turbulent kinetic energy derived from the analysis of HALO in-situ data along sublegs with different lengths. (b) Energy dissipation rate (EDR) for all wind components in an aircraft-related coordinate system and the geometric mean of EDR calculated from all wind components.

On that day, mountain wave (MW) excitation and propagation was favoured by the alignment of strong surface winds and the polar front jet. A combination of in-situ observations, ECMWF and empirical turbulence forecasts, and high resolution simulations was applied to characterize the observed turbulent event (see Fig. 1 for the in-situ data analysis). From the in situ observations, maximum EDR values (cubic root of the energy dissipation rate) of 0.39 $m^{2/3} s^{-1}$ are obtained, which correspond to moderate to severe turbulence for a medium-weight aircraft such as HALO. These show that a pronounced negative vertical shear of the horizontal wind favoured overturning and breaking of MWs in the area of the encountered turbulence. The turbulent region was tilted upstream and extended over a vertical range of about 2 km. The data analyses in concert with the high-resolution numerical simulations suggested that HALO was flying through the centre of a breaking MW field while the French Falcon encountered the lower edge of this region. Surprisingly, the pronounced gradients in the horizontal wind speeds leading to the deactivation of the automatic thrust control were located north of the breaking MW field. In this area, our analysis suggests the presence of gravity waves which could have generated the encountered modulation of the horizontal wind field.

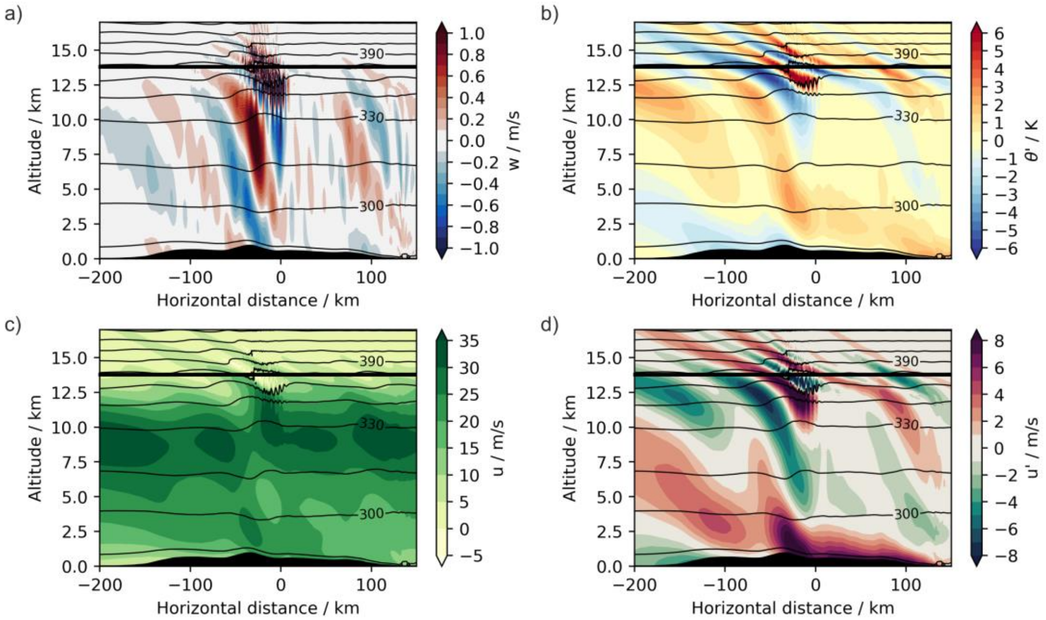

Figure 2: Idealized EULAG simulations after 3 h of the (a) vertical wind speed, (b) potential temperature fluctuations, (c) horizontal wind speed and (d) perturbation of the horizontal wind speed. Black contour lines are isentropic surfaces and the thick black line shows the altitude of HALO's flight track.

Idealized two-dimensional numerical simulations (Fig. 2) indicate that the turbulence was generated by overturing, convectively unstable mountain waves near the tropopause in the lee of the mountains. In a more detailed study by Wilms et al., 2019, the generation of turbulence along the flight path is further studied through three-dimensional numerical simulations in combination with the aircraft in-situ observations. As in the 2D numerical simulations, the turbulent region is characterized by large-amplitude vertical wind fluctuations which coincide locally with a stagnation of the horizontal flow.

The peculiarity of this case is that the strong turbulence occurred downstream and in between the two Icelandic mountains Hofsjökull and Langjökull. High-resolution numerical simulations of this case by H. Wilms, with realistic and idealized topography, show that the flow over these two nearby mountains is responsible for the observed turbulence. The hydrostatic mountain waves excited by each of these mountains not only propagate vertically into the stratosphere as already shown in Fig. 2. They also disperse horizontally in ship-wave like patterns. In the region downstream and in between Hofsjökull and Langjökull, both wave trains interfere and their superposition leads to enhanced amplitudes and, eventually, to convective instabilities. By comparing numerical results from simulations with only one of the mountains with the simulation with both mountains, the wave interference amplified the turbulence intensity by a factor of five and doubled the vertical extent of the turbulent region.

Deep Propagating Waves over Auckland Islands

T. Mixa has undertaken a reanalysis of a ship wave GW propagation event observed over Auckland Island during the 2014 DEEPWAVE campaign (see Fritts et al., 2016). The initial observations (Pautet et al., 2016) indicated a GW with a 40 km horizontal wavelength (λ_x) and temperature perturbations measured at ±10 K at an altitude of 87 km (see Figure 3a). Eckermann et al., 2016 analysed this event using a linear Fourier ray model, using NAVGEM (Eckermann et al., 2018) reanalysis profiles of wind and temperature (Fig. 3b) to reproduce the dominant GW characteristics observed at 87 km (Fig. 3c), estimating the resulting GW drag of 300-600 $m^2 s^{-2}$ at the GW breaking altitude.

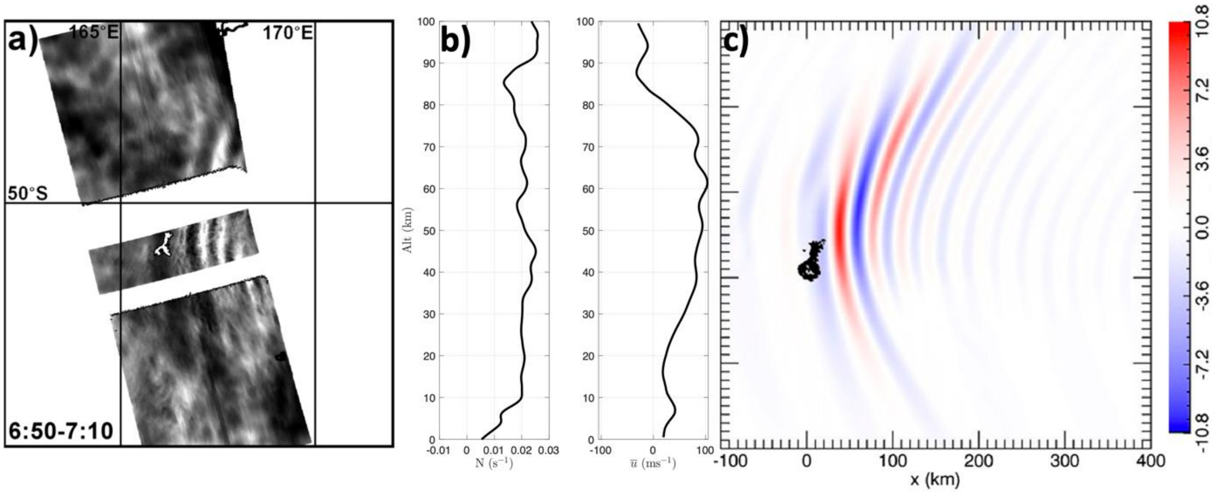

Figure 3: Initial AMTM GW observations from Pautet et al., 2016 at 87 km (a), NAVGEM vertical temperature and wind profiles (b), and simulation results from Eckermann et al., 2016 at 87 km (c).

The linear ray tracing model used by Eckermann et al., 2016 had several critical limitations motivating a reanalysis with EULAG. Linear ray propagation assumes a steady-state background atmosphere with instantaneous GW propagation from the source to the parameterized breaking altitude. The scheme traces individual ray paths from broad spectrum of GWs initialized at the ground and identifies the characteristics at 87 km based on the breaking altitude of each mode, with the approximate propagation time determined by each mode's vertical group velocity. As a linear model, this mechanism does not account for wave-wave interaction between different frequencies of GWs - GW frequencies and wavelengths cannot change with space or time, all modes propagate independently of each other, and breaking altitudes are estimated with saturation amplitudes rather than fully characterized. Crucially, the results in Eckermann et al., 2016 removed GW spectral components undergoing vertical reflections, resonance, and evanescent tunneling to evaluate purely propagating modes.

Description of Simulation Setup

In light of these limitations, the event has been reanalysed using the EULAG model to evaluate the GW propagation and breaking characteristics without removing any dynamics or spectra. EULAG simulations were run in a fully nonlinear, compressible, 2D configuration with 200 m grid resolution. The background wind and temperature profiles are initialized from NAVGEM reanalysis data with GW forcing generated by the Auckland Island terrain using ASTER topography data. Simulations employ a 288 km streamwise domain with altitudes up to 100 km to accommodate lateral (nonhydrostatic) propagation and characterize GW drag above the instabilities observed at 87 km. The vertical sponge is designed to replicate the behaviour of molecular viscosity with altitude and has the advantage of not requiring the specification of a damping region near the upper boundary.

Overview of Results

The 2D GW perturbation characteristics are shown in Figure 4 at 58 minutes elapsed time. To account for horizontal variability of the wave characteristics, Perturbations are calculated by subtracting a local background averaged over the dominant horizontal wavelet scale at each point in space and time. The GW propagation characteristics vary significantly in both the vertical and the spanwise directions. GW phase tilt indicates propagation characteristics in the troposphere immediately above the terrain, a region of evanescence over the stratospheric jet, and propagation characteristics again between the jet maximum and the critical level at 82 km. Near the stratospheric jet, GW phase structure indicates upward propagation directly over the terrain, horizontal propagation immediately in the lee of the mountain, and downward propagation farther downstream.

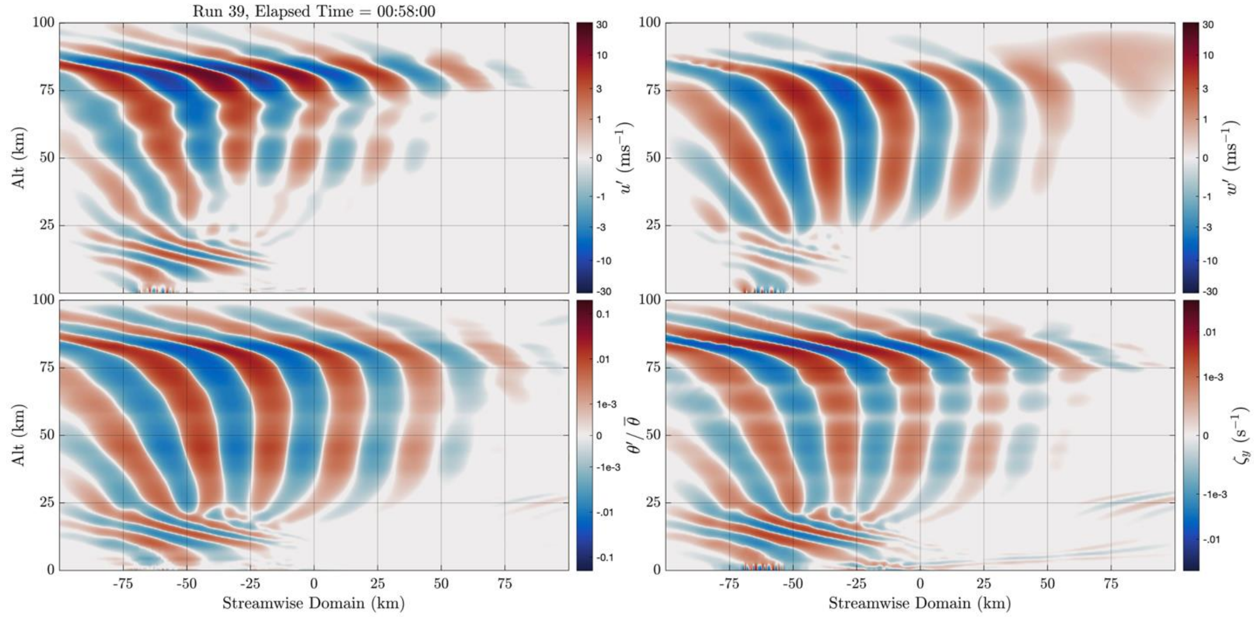

Figure 4: GW perturbations of horizontal velocity, vertical velocity, normalized potential temperature, and vorticity.

The GW flux characteristics shown in Figure 5 confirm the propagation characteristics identified in Figure 4. Horizontal flux of vertical momentum (MF_x) plots show vertical propagation through the jet, indicating GW tunneling as the dominant propagation mechanism for waves reaching 87 km. Downward propagation east of x = -20 km is shown by both the MF_x and the vertical energy flux (EF_z). Long horizontal bands in the horizontal energy flux EF_x also indicate several regions of ducting.

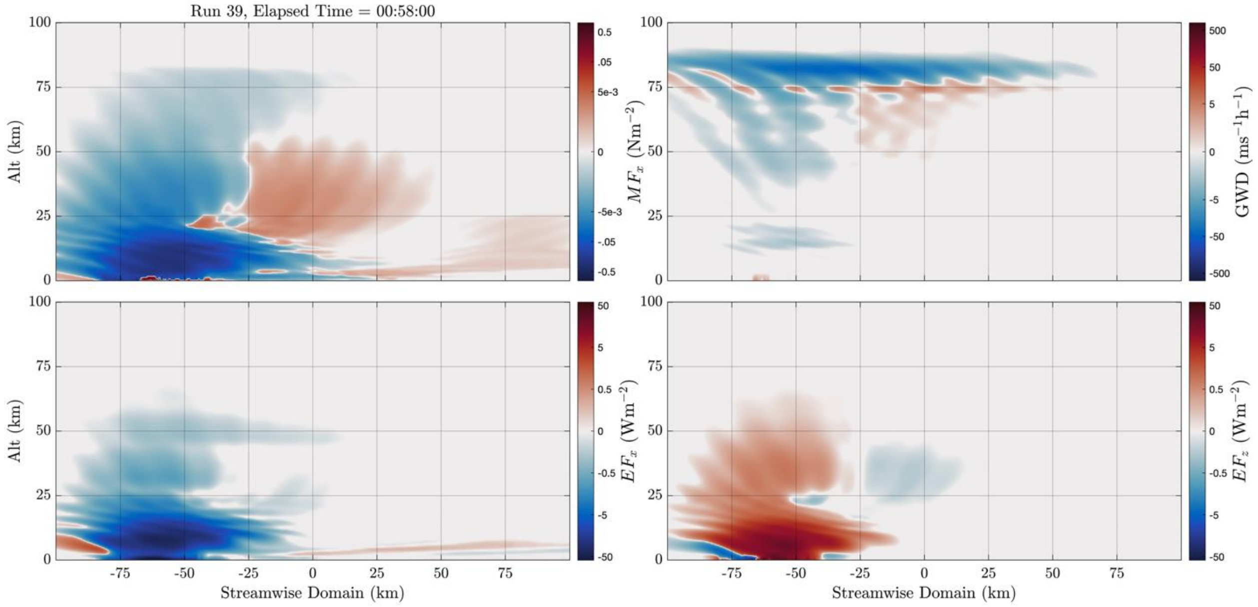

Figure 5: GW momentum flux, gravity wave drag, horizontal energy flux, and vertical energy flux.

Figure 6 shows vertical profiles of the GW horizontal wavelength and intrinsic frequency at five horizontal locations in the domain. At all locations, λ_x increases as the GW propagates through the stratospheric jet, agreeing with the observed 40 km horizontal wavelength at 87 km altitudes even though λ_x is smaller at lower altitudes. In the jet region, smaller λ_x (and consequently, larger ω_i) occur farther downstream of the topography, producing GW reflection farther in the lee of the mountains as the GW is unable to penetrate the deeper evanescent region.

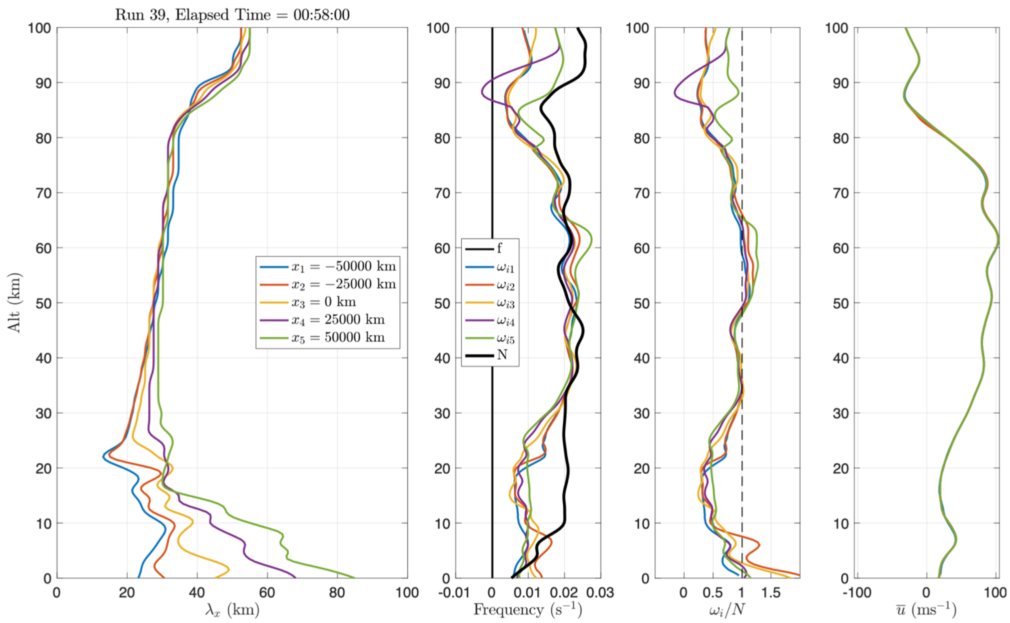

Figure 6: Vertical Profiles of λ_x, ω_i, ω_i/N, and background wind at the five specified horizontal locations in the domain.

Preliminary Conclusions and Future Plans

The results of this study show several unique characteristics that disagree with the original analysis presented in Eckermann et al., 2016. Evanescent tunneling is shown to be the dominant propagation mechanism of

GWs penetrating the stratospheric jet to reach the mesosphere, whereas the GW characterized by Eckermann et al., 2016 does not encounter an evanescent region. The fast propagation time of the evanescent tunneling GW, under an hour from initialization, further indicates that the cutoff times used by Eckermann et al., 2016 give an inaccurate picture of the event. While GWs in this simulation have a 40 km λ_x at 87 km, the wavelength changes with altitude, unlike the Eckermann et al., 2016 result which requires that a 40 km λ_x GW in the mesosphere must be triggered with the same λ_x at the ground. Future studies (currently in progress) will evaluate the 3D characteristics of the event to discern the dominant instability mechanism and the resulting GW drag distribution.

References:

Bramberger, M., A. Dörnbrack, H. Wilms, F. Ewald, and R. Sharman, 2019: Mountain Wave Turbulence Encounter of the Research Aircraft HALO above Iceland, *J. Appl. Met. Clim*., submitted 31 March 2019, minor revisions, resubmitted 6 September 2019

Eckermann, S.D., D. Broutman, J. Ma, J.D. Doyle, P. Pautet, M.J. Taylor, K. Bossert, B.P. Williams, D.C. Fritts, and R.B. Smith, 2016: Dynamics of Orographic Gravity Waves Observed in the Mesosphere over the Auckland Islands during the Deep Propagating Gravity Wave Experiment (DEEPWAVE). *J. Atmos. Sci.*, **73**, 3855–3876.

Eckermann, S.D., J. Ma, K.W. Hoppel, D.D. Kuhl, D.R. Allen, J.A. Doyle, K.C. Viner, B.C. Ruston, N.L. Baker, S.D. Swadley, T.R. Whitcomb, C.A. Reynolds, L. Xu, N. Kaifler, B. Kaifler, I.M. Reid, D.J. Murphy, and P.T. Love, 2018: High-Altitude (0–100 km) Global Atmospheric Reanalysis System: Description and Application to the 2014 Austral Winter of the Deep Propagating Gravity Wave Experiment (DEEPWAVE). *Mon. Wea. Rev.*, **146**, 2639–2666.

Fritts, D.C., R.B. Smith, M.J. Taylor, J.D. Doyle, S.D. Eckermann, A. Dörnbrack, M. Rapp, B.P. Williams, P. Pautet, K. Bossert, N.R. Criddle, C.A. Reynolds, P.A. Reinecke, M. Uddstrom, M.J. Revell, R. Turner, B. Kaifler, J.S. Wagner, T. Mixa, C.G. Kruse, A.D. Nugent, C.D. Watson, S. Gisinger, S.M. Smith, R.S. Lieberman, B. Laughman, J.J. Moore, W.O. Brown, J.A. Haggerty, A. Rockwell, G.J. Stossmeister, S.F. Williams, G. Hernandez, D.J. Murphy, A.R. Klekociuk, I.M. Reid, and J. Ma, 2016: The Deep Propagating Gravity Wave Experiment (DEEPWAVE): An Airborne and Ground-Based Exploration of Gravity Wave Propagation and Effects from Their Sources throughout the Lower and Middle Atmosphere. *Bull. Amer. Meteor. Soc.*, **97**, 425–453.

Pautet, P.-D., Taylor, M. J., Fritts, D. C., Bossert, K., Williams, B. P., Broutman, D., Ma, J., Eckermann, S. D., and Doyle, J. D. (2016), Large-amplitude mesospheric response to an orographic wave generated over the Southern Ocean Auckland Islands (50.7°S) during the DEEPWAVE project, *J. Geophys. Res. Atmos.*, 121, 1431– 1441.

Schäfler, A., G. Craig, H. Wernli, P. Arbogast, J.D. Doyle, R. McTaggart-Cowan, J. Methven, G. Rivière, F. Ament, M. Boettcher, M. Bramberger, Q. Cazenave, R. Cotton, S. Crewell, J. Delanoë, A. Dörnbrack, A. Ehrlich, F. Ewald, A. Fix, C.M. Grams, S.L. Gray, H. Grob, S. Groß, M. Hagen, B. Harvey, L. Hirsch, M. Jacob, T. Kölling, H. Konow, C. Lemmerz, O. Lux, L. Magnusson, B. Mayer, M. Mech, R. Moore, J. Pelon, J. Quinting, S. Rahm, M. Rapp, M. Rautenhaus, O. Reitebuch, C.A. Reynolds, H. Sodemann, T. Spengler, G. Vaughan, M. Wendisch, M. Wirth, B. Witschas, K. Wolf, and T. Zinner, 2018: The North Atlantic Waveguide and Downstream Impact Experiment. *Bull. Amer. Meteor. Soc*., **99**, 1607–1637.

Wilms, H., Bramberger, M., and A. Dörnbrack, 2019: Observation and Simulation of Mountain Wave Turbulence above Iceland: Turbulence Intensification due to Wave Interference; in preparation.